Heat Mass Transfer (2011) 47:703–717
DOI 10.1007/s00231-011-0761-4

ORIGINAL

Evaporation flow pattern and heat transfer of R-22 and R-134a in small diameter tubes

Hoo-Kyu Oh · Chang-Hyo Son

Received: 21 May 2010 / Accepted: 5 January 2011 / Published online: 22 January 2011

Abstract The flow patterns and heat transfer coefficients of R-22 and R-134a during evaporation in small diameter tubes were investigated experimentally. The evaporation flow patterns of R-22 and R-134a were observed in Pyrex sight glass tubes with 2 and 8 mm diameter tube, and heat transfer coefficients were measured in smooth and horizontal copper tubes with 1.77, 3.36 and 5.35 mm diameter tube, respectively. In the flow patterns during evaporation process, the annular flows in 2 mm glass tube occurred at a relatively lower vapor quality compared to 8 mm glass tube. The flow patterns in 2 mm glass tube did not agree with the Mandhane's flow pattern maps. The evaporation heat transfer coefficients in the small diameter tubes ($d_i < 6$ mm) were observed to be strongly affected by tube diameters, and to differ from those in the large diameter tubes. The heat transfer coefficients of 1.77 mm tube were higher than those of 3.36 mm and 5.35 mm tube. Most of the existing correlations failed to predict the evaporation heat transfer coefficient in small diameter tubes. Therefore, based on the experimental data, the new correlation is proposed to predict the evaporation heat transfer coefficients of R-22 and R-134a in small diameter tubes.

List of symbols

d	Diameter of tube (m)
dz	Length of subsection (m)
f	Two-phase multiplier
G	Mass flux (kg m^{-2} s^{-1})
h	Heat transfer coefficient (kW m^{-2} K^{-1})
i_{fg}	Latent heat (kJ kg^{-1})
i	Enthalpy (kJ kg^{-1})
ID	Inner diameter (m)
j	Superficial velocity (m s^{-1})
k	Thermal conductivity (W m^{-1} K^{-1})
L	Total evaporation length, test section length (m)
N	Number of data
M	Mass flow rate (kg h^{-1})
q	Heat flux (kW m^{-2})
Q	Heat capacity (kW)
T	Temperature (K)
x	Vapor quality
z_{sc}	Subcooled length

Greek symbols

Δ	Difference
μ	Dynamic viscosity (Pa s)
ρ	Density (kg m^{-3})
X_{tt}	Martinelli parameter

Subscripts

avg	Average
abs	Absolute
cal	Calculated
e	Evaporation
exp	Experimental
f	Saturated liquid
g	Saturated gas
i	Inner diameter
in	Inlet
l	Liquid
L	Local
OD	Outer diameter
out	Outlet
r	Refrigerant
sat	Saturation

H.-K. Oh · C.-H. Son (✉)
Department of Refrigeration and Air-Conditioning Engineering, College of Engineering, Pukyong National University, San 100, Yongdang-dong, Nam-gu, Pusan 608-739, South Korea
e-mail: sonch@pknu.ac.kr

t Turbulent
TP Two-phase
w Wall
wi Inside wall
wo Outside wall

1 Introduction

The studies for alternative refrigerants have been carried out actively from 1980s because of the use restriction of CFCs and HCFCs refrigerants, and the researches for heat exchanger with high efficiency have been also done together. Among these researches, it is very peculiar to apply small diameter tubes ($d_i < 6$ mm) to heat exchanger. Large diameter tubes have been used until comparatively lately. However, small diameter tubes have been largely used these days because of many merits [1, 2]. The design guide of heat exchanger is rightly changed, if working fluids in it become different. Therefore, recently many researches tend to focus on carrying out studies for alternative refrigerants and heat exchanger with small diameter tubes together. So, the main studies for alternative refrigerants are highly related to the studies for heat exchanger with small diameter tubes. Some examples of the most productive literatures are briefly described as follows:

Oh et al. [3] investigated experimentally heat transfers of R-134a in small diameter tubes of 0.75 and 1.0 mm. They reported that the heat transfer in the forced convection region was more influenced by the mass flux than by Boiling number. In addition, they proposed the new correlation for convective heat transfer in small diameter tubes. In addition, their results indicate that the evaporation heat transfer characteristics in small diameter tubes differ from those in large diameter tubes.

Tran et al. [4] studied the local boiling heat transfer coefficient of R-12 and R-113 flowing in a single circular tube ($d_i = 2.46$ mm) and rectangular channel ($d_i = 2.40$ mm). Their results showed that there was no significant geometry effect for the two channels tested. The heat transfer coefficient was dependent on the heat flux and independent on mass flux and vapor quality.

Bao et al. [5] experimentally studied the flow boiling heat transfer of R-11 and R-123 in a smooth copper tube of a 1.95 mm inner diameter. They concluded that the boiling heat transfer coefficient was a strong function of the heat flux and system pressure, while the effects of the mass flux and vapor quality were very small. The heat transfer coefficients for R-11 and R-123 are slightly different under the same test conditions.

Haynes and Fletcher [6] experimentally studied the subcooled and saturated flow boiling of R-11 and R-123 through 0.95 and 1.95 mm inner diameters. They concluded that the nucleate component becomes more important and ultimately dominates as the subcooled liquid approaches saturation, especially if the heat flux is high or the fluid mass flux is low. They also proposed a correlation for subcooled boiling.

Zhang et al. [7] analyzed the existing correlation for flow boiling heat transfer in minichannels. They concluded that most of the existing correlations for boiling heat transfer are developed by being based on the Chen [8] correlation and developed under liquid-turbulent and gas-turbulent flow conditions, and that it is therefore inconsistent to use them under other flow conditions. In comparison with the collected database, the correlations of Chen [8], Liu and Winterton [9] and Kandlikar [10] work well for saturated flow boiling in minichannels.

Choi et al. [11, 12] investigated the convective boiling heat transfer coefficient of R-22, R-134a, and CO_2 in horizontal minichannels with inner diameters of 1.5 and 3.0 mm constructed of stainless steel tube and a length of 2 m. They found that the average heat transfer coefficient ratio of R-22:R-134a:CO_2 was approximately 1.0:0.8:2.0. They also proposed a heat transfer coefficient correlation based on the superposition model for refrigerants in minichannels.

Yan and Lin [13] performed an experimental investigation into the evaporation heat transfer coefficient and pressure drop of R-134a in a tube with an inner diameter tube of 2 mm. They found that at a higher wall heat flux the evaporation heat transfer coefficient was higher except in the high vapor quality region and reverse results in the case of the high vapor quality region for a high wall heat flux. They found that the heat transfer coefficient of small tubes is higher than that of conventional tube ($d_i > 8$ mm) around 30–80%.

The recent review on the two phase flow and boiling heat transfer in microchannels is conducted by Fujita et al. [14], Kim et al. [15], Ghiaasiaan andAbdel-khalik [16], Thome [17], Sobhan and Garimella [18], Kandlikar [10, 19], Watel [20], Yun et al. [21], Lee and Mudawar [22], Cavallini et al. [23] and Vlasie et al. [24].

The above literature review clearly indicates that the experimental data for the evaporation heat transfer of the HFC refrigerants in small tubes are still in urgent need. Despite worthwhile an application in industry, relatively little information is currently available from experimental work on heat transfer and flow characteristics in small tubes.

As a consequence, in the present study evaporation flow patterns were observed in horizontal Pyrex sight glass tubes of 2 and 8 mm, respectively. Also, the evaporation heat transfer coefficients of R-22 and R-134a were measured in smooth horizontal copper tubes with 1.77, 3.36 and

5.35 mm, respectively. The effects of the mass flux, heat flux, and saturation temperature of R-22 and R-134a on the heat transfer coefficient and friction factor are presented. In addition, a correlation for predicting heat transfer coefficient is proposed for practical applications.

2 Experimental apparatus and procedures

2.1 Test facility

Figure 1 shows the schematic of the experimental apparatus. The test facility consists of two main parts: a refrigerant loop and a water loop. Detailed descriptions of the two test parts of the test facility are provided below. A schematic diagram of the test rig and Pyrex sight glass tube is shown in Fig. 2.

2.1.1 Refrigerant loop

The refrigerant loop contains a magnetic gear pump, a mass flow-meter, an evaporator, a test section, a subcooler and a receiver etc. The subcooled refrigerant is charged in the receiver where it is further cooled to increases its density. The refrigerant liquid in the receiver is circulated by a magnetic gear pump, and then flows through a flow-meter. The liquid of refrigerant enters the evaporator, where it is heated up to the desired temperature of the test section. Electrically insulated heating wires are wrapped around the surface of copper tubes in the evaporator. The evaporator is insulated with glass fibers and rubber. The amount of heat loss from the evaporator is calibrated through pretests with water; this is the correlated to the voltage input. In passing through the condenser, the two-phase refrigerant is completely condensed and subcooled by cooling water.

Afterwards, the refrigerant is subcooled by the additional heat exchanger and goes into the liquid receiver. Finally, the subcooled refrigerant is recirculated through the refrigerant loop. The subcooler is a counterflow heat exchanger with refrigerant flowing in the inner tube and the water flowing in the annulus. It is used to condense the refrigerant leaving the condenser. The mass flow rate of refrigerant into the test section is adjusted by changing the speed of the gear pump. The refrigerant flow rate is measured by the mass flow-meter. The pressure of the cycle is controlled by the charged amount of refrigerant.

2.1.2 Water loop

The water loop is composed of a centrifugal pump, an in-line electric heater and a heat exchanger. The cooling water is pumped to the circular-tube annulus, where it absorbs the heat of the condensing refrigerant. The mass flow rate of cooling water is controlled by adjusting the metering valve and pump speed. The inlet temperature of the cooling water at the test section is controlled by both the electric heater and the refrigeration unit. The mass flow rate of cooling water is also measured by a turbine type flow meter.

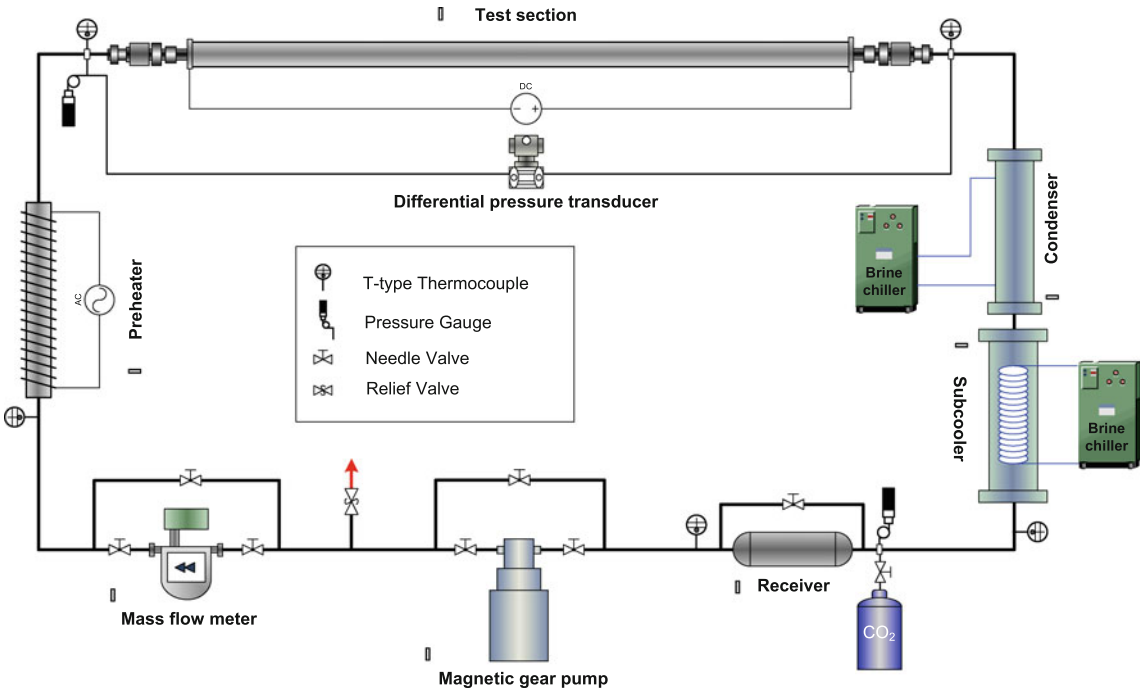

Fig. 1 Schematic diagram of experimental apparatus

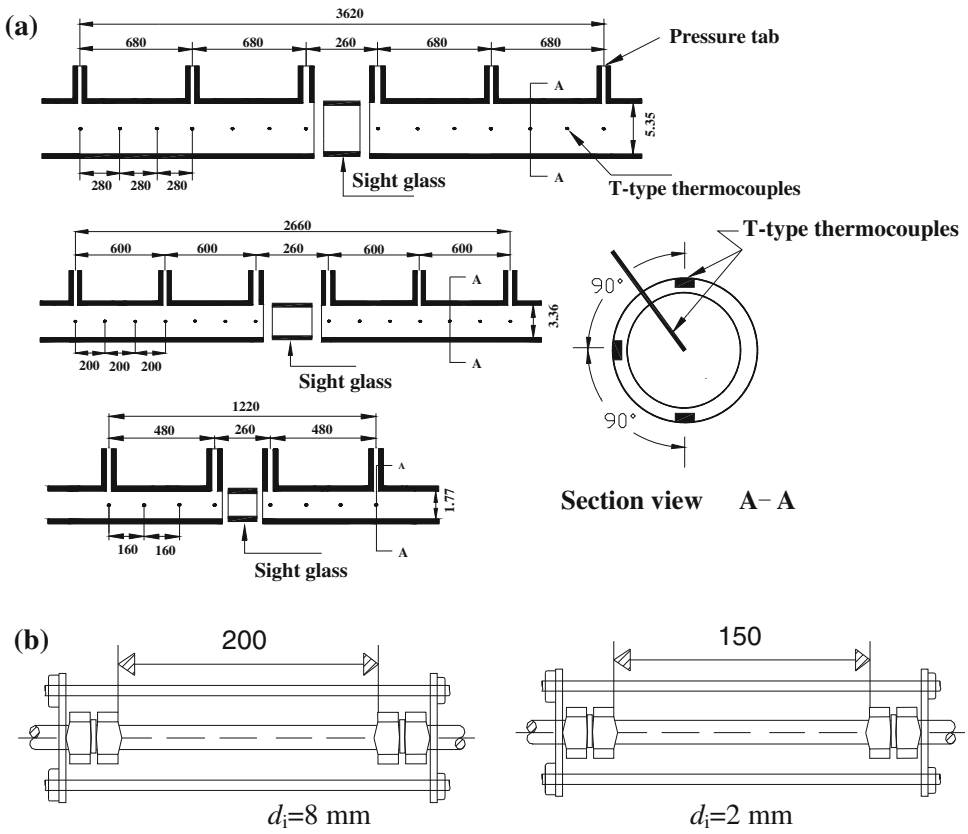

Fig. 2 Schematic diagram of test section and Pyrex sight glass tube. **a** Test section and **b** Pyrex sight glass tube

2.2 Test section

Figure 2a shows the schematic drawings of the test section which is a horizontal and smooth tube-in-tube type heat exchanger. The refrigerant flows through the inside of copper tube and the cooling water flows through the annulus in the counterflow direction. The tubing of the refrigerant loop is made of smooth copper tube with internal diameters of 1.77, 3.36 and 5.35 mm. All copper tubes have 0.7 mm tube wall thickness. The evaporator length is 1,220, 2,660 and 3,620 mm, respectively and contains subsections along with 160, 200 and 260 mm in length of one subsection. The outer tube is made of a clear polyvinyl chloride (PVC) tube. Sight glass is mounted at the middle and outlet of test section to visualize the refrigerant flow.

Figure 2b shows the schematic diagram of Pyrex sight glass tube with inner diameters of 2 and 8 mm. The test section is insulated by using a rubber to minimize heat exchange to ambient. Temperature, pressure and mass flow rates are measured during the tests as follows:

2.2.1 Temperature

Three types of temperature sensor are used in the experiment. The refrigerant temperatures are measured by T-type thermocouples ($d_i = 0.5$ mm) at the inlet and outlet of each subsection. The temperature of cooling water at the inlet and outlet of subsection are measured using Pt 100 sensors in order to determine the heat transfer rate in the test section. T-type fine thermocouples with a tip diameter 0.1 mm are soldered onto the copper tube's surface to measure the wall temperature of the top, side and bottom of test tube.

2.2.2 Pressure

The pressure at the inlet and outlet of each subsection is measured with a pressure transducer. The pressure drop of the test section is obtained from the difference of measured pressure at the inlet and outlet. According to the calibration before shipment, its divergence with standard value is found less than 0.001 MPa over the full measurement scale.

2.2.3 Mass flow rate

Mass flow rate of the refrigerant is measured with the mass flow meter of Oval corporation, and mass flow rate of the cooling water is measured with the flow meter of Schlumberger corporation.

2.2.4 Instrument calibration

The mass flow meter utilizing the Coriolis principle was calibrated by running water at different flow rates and weighing the amount of water flowing in a given time period. The turbine flow meter was done in the same way except that the water was used as the calibration fluid. The RTDs and thermocouples were calibrated in a refrigerated temperature bath. The pressure transducer was calibrated against a calibrated (reference) dial pressure gauge. The watt transducers were checked by measuring the voltage and current and comparing them with the signal output. Table 1 lists the instrument specifications for the condensation heat transfer test.

2.3 Experimental procedure

As mentioned above, the test rig can be used to conduct the evaporation heat transfer test. The physical properties of refrigerants under test were incorporated in the data-acquisition system consisting of a data logger, interface card (HPIB), and a compatible PC. The data was analyzed in real time using PC and a data reduction program (MS-Excel with a Visual Basic for Applications). All of the information about the test conditions and data were displayed on the monitor during the test. The test conditions were changed based on this information. All channels in the data-acquisition system were scanned five times and then averaged. The data collection took about 2 min for each run. The system was allowed to come to steady state before any data were recorded. The test conditions in this study are summarized in Table 2.

2.4 Data reduction

The local heat transfer coefficient in evaporation process could be evaluated by the following Eq. 1:

$$h_{e,loc} = \frac{q_e}{T_{e,w,i} - T_e} \tag{1}$$

where $h_{e,loc}$ represents the local heat transfer coefficient in subsection of evaporator, T_e, is the bulk refrigerant temperature, and $T_{e,w,i}$ is the inner wall temperature calculated from the measured outside wall temperature, T_w, using the equation of radial thermal conduction through the wall.

$$T_{e,w,i} = T_w - \frac{Q_{e,sub} \cdot \ln \frac{d_o}{d_i}}{2\pi \cdot k_w \cdot dz} \tag{2}$$

where $Q_{e,sub}$ is the input heat capacity of each section, d_i and do are the inner and outer diameter of the copper tube, respectively, dz is the length of subsection. T_w is the average temperature of the top, both the left and right sides and the bottom wall.

$$T_w = \frac{T_{w,top} + T_{w,right} + T_{w,left} + T_{w,bottom}}{4} \tag{3}$$

where $T_{w,top}$, $T_{w,right}$, $T_{w,left}$ and $T_{w,bottom}$ are the measured temperature at the top, both the left and right sides and bottom wall, respectively.

The quality, x, at the measurement location, z, is determined based on thermodynamic properties.

$$x = \frac{i - i_f}{i_{fg}} \tag{4}$$

The refrigerant flow is not completely saturated at the

Table 2 Test conditions for evaporation heat transfer

Refrigerant	R-22	R-134a
Mass flux of refrigerant (kg m^{-2} s^{-1})	200–600	
Inner diameter tube of test section (mm)	1.77, 3.36, 5.35	
Saturated temperature of refrigerant (°C)	0, 5	
Heat flux (kW m^{-2})	5–30	

Table 1 Instrument specification used in this study

Item	Range	Accuracy
T-type thermocouple	−200 to 350°C	±0.1°C
T-type fine thermocouple	−200 to 200°C	±0.01°C
Pt 100 sensor	−200 to 400°C	±0.05°C
Pressure transducer	0–1379 kPa	±0.1% FS
	0–4826 kPa	±0.1% FS
Differential pressure transducer	0–69 kPa	±0.1% FS
Coriolis mass flow meter	0–4.54 kg min	±0.24% FS
Watt transducer	0–5 kW	±0.2%
Turbine flow meter	0–9.5 l/min	±0.15% FS
RTD	−200 to 480°C	±0.05°C

inlet of the test section. Even though it is just short, it is necessary to find the subcooled length for data reduction accuracy. The subcooled length is calculated using the following equation to find the initial point of saturation.

$$z_{sc} = L\frac{i_f - i_{f,in}}{\Delta i} = L\frac{i_f - i_{f,in}}{Q/M} \quad (5)$$

The outlet quality is then found using the following equation.

$$x_{out} = \frac{\Delta i + i_{f,in} - i_f}{i_{fg}} \quad (6)$$

The saturation pressure at the initial point of saturation is then determined by interpolation of the measured pressure and the subcooled length. In this study, all refrigerant properties are calculated by REFPROP (version 8.01) made by NIST (National Institute of Standards and Technology) [25].

The results from the present uncertainty analysis for the experiments are summarized in Table 3. The maximum uncertainty of heat transfer coefficient is ±13.5% at typical test conditions without oil, which is estimated based on the analysis of error propagation reported by Moffat [26].

3 Results and discussion

3.1 Evaporation flow patterns

3.1.1 Evaporation flow patterns inside horizontal tubes of 2 and 8 mm

Figure 3 presents the measured evaporation flow patterns of R-22 with mass flux in 2 mm tube. Table 4 shows the experimental conditions for two-phase flow patterns during evaporation.

As shown in Fig. 3, wavy and wavy-annular flow is observed at high mass fluxes (Fig. 3 right). At lower mass fluxes the wavy, wavy-annular, annular flow is observed, respectively. In Fig. 3, there is an effect of the mass flux on the transition boundaries. The quality for transition of wavy flow and wavy-annular flow is lower for the higher mass flux. This is due to higher difference of vapor and liquid velocity with increasing mass flux at the same quality. From the experimental results observed in 2 mm tube, wavy-annular and annular flow is predominant at lower and higher mass flux, respectively. Here a large region of wavy-annular and annular flow is found.

Figure 4 shows the flow patterns of R-134a in 2 and 8 mm tube at mass flux of 200 kg m^{-2} s^{-1}. From the experimental result in 2 mm wavy, wavy-annular, annular flow is observed at 0.1, 0.3 and 0.7 quality, respectively. Annular flow occurs clearly at the vapor quality of $x > 0.5$. The results in 8 mm tube show that stratified and wavy flow is observed at 0.1 and 0.3–0.7, respectively. Wavy flow appears evidently at $x > 0.5$. Therefore, it can be seen that the quality for wavy, wavy-annular and annular flow in 2 mm is lower than that in an 8 mm. And smaller diameter tube becomes thinner liquid film of annular flow. This is because of the higher shear stress due to an increase in vapor velocity at the vapor–liquid interface.

Figure 5 presents the flow patterns of R-22 and R-134a in 2 mm tube at the mass flux of 400 kg m^{-2} s^{-1}. The flow pattern of R-22 is slightly different from that of R-134a at the quality of 0.1. But at all the qualities, R-22 and R134a in 2 mm tube are almost similar flow patterns. Therefore, from the above experimental results, it can be seen that the evaporation flow patterns have an affect on more inner tube diameter than fluid property.

Table 3 Parameters and estimated uncertainties

Parameters	Uncertainty (%)
Temperature (°C)	±0.2
Water flow rate (kg s)	±1.5
Mass flux of refrigerant (kg m^{-2} s^{-1})	±1.7
Heat transfer rate of test section (kW)	±3
Vapor quality (–)	±5.87
Two-phase heat transfer coefficient, (kW/m^2k)	±13.5

3.1.2 Comparison of experimental data with existing flow pattern maps

Flow patterns are very important in understanding the complex two-phase flow phenomena and heat transfer characteristics in flow evaporation. To predict the local flow patterns in a tube, flow pattern map is generally used. In fact, numerous flow patterns based flow boiling heat transfer have been proposed in the years for predicting two-phase flow patterns in horizontal tubes, such as those by Baker [27], Scott [28], Mandhane et al. [29], Taitel and Dukler [30], Bennett [31], Bergles et al. [32], Wambsganss et al. [33] and Dobson et al. [34].

The maps of Baker [27], Scott [28], Mandhane et al. [29] and Taitel and Dukler [30] were proposed for adiabatic conditions. Some other maps are those of Bennett [31], Bergles et al. [32], Breber et al. [35], Tandon et al. [36] and Cavallini et al. [23] for evaporation. Specifically, adiabatic flow patterns in small diameter tubes have been proposed by Wambsganss et al. [33] and by Dobson et al. [34].

However, none of these is applicable to evaporation in small diameter tubes because the two-phase flow characteristics of evaporation are greatly affected by inner diameter of tube. Therefore, a flow pattern map covering a

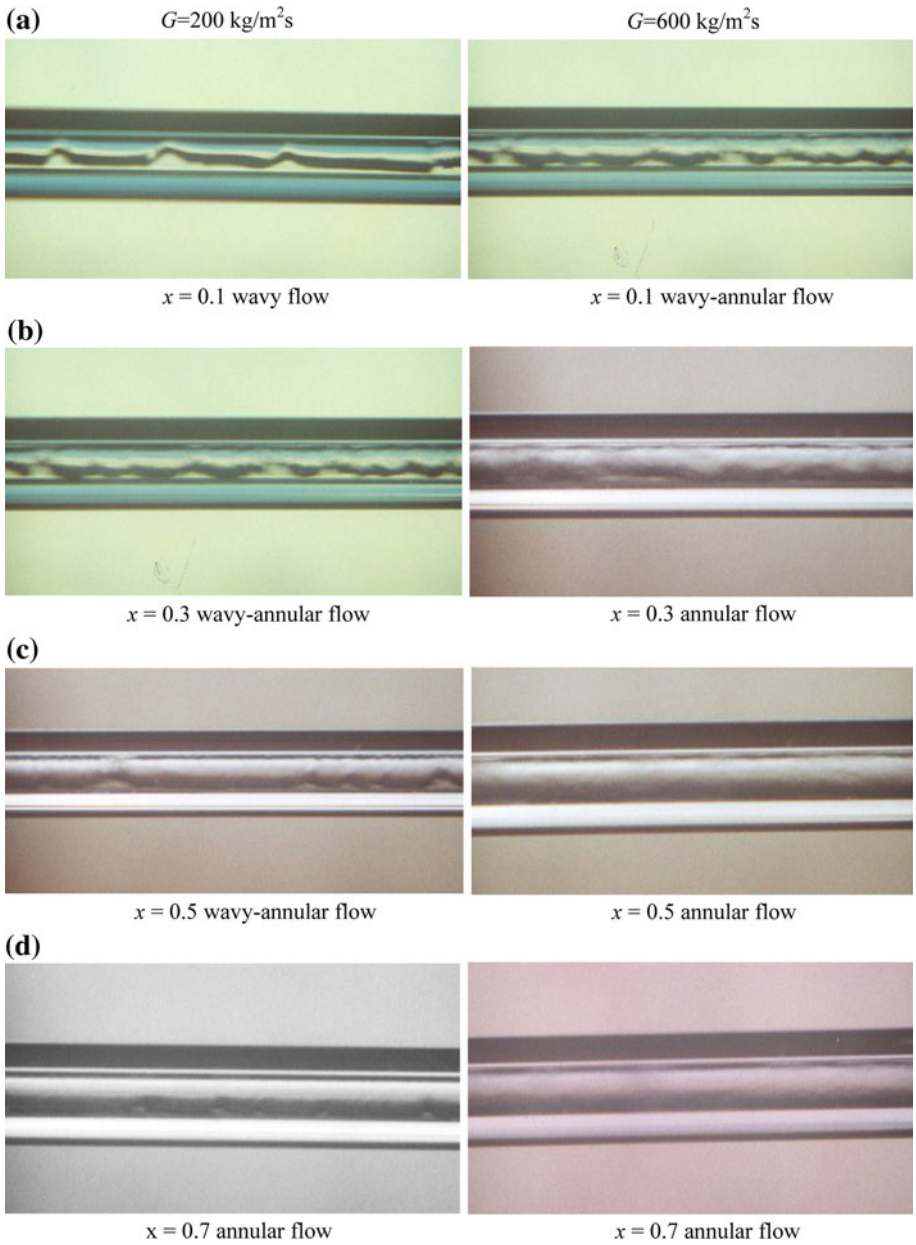

Fig. 3 Experimental flow patterns for R-22 in 2 mm tube

Table 4 Experimental conditions for evaporation flow patterns

Refrigerant	R-22	R-134a
Quality (/)	0–1	
Refrigerant mass flux (kg m^{-2} s^{-1})	100–600	
Inner diameter tube of test section (mm)	2, 8	
Saturated temperature of refrigerant (°C)	0, 5	

wider range of parametric conditions is needed to accurately predict the flow patterns for evaporation in small diameter tubes.

In this study, the maps of Mandhane et al. [29] and Taitel and Dukler [30] proposed in conventional tube, and of Dobson et al. [34], which is very similar to the test conditions of this study, are compared with experimental data.

3.1.2.1 Mandhane' flow pattern map Figure 6 shows the flow pattern map evaluated for R-22 in internal diameter tube of 2 mm, plotted on the Mandhane's flow map. (Flow pattern legend: A is annular flow, W–A is wavy-annular flow, W is wavy flow.) A solid line in Fig. 6 is the transition boundaries for flow patterns. From the experimental results in Fig. 6, wavy flow and annular flow occurs at the superficial velocities of gas lower than those shown on the present map. At the present test conditions slug flow, plug flow and stratified flow do not occur and then wavy flow

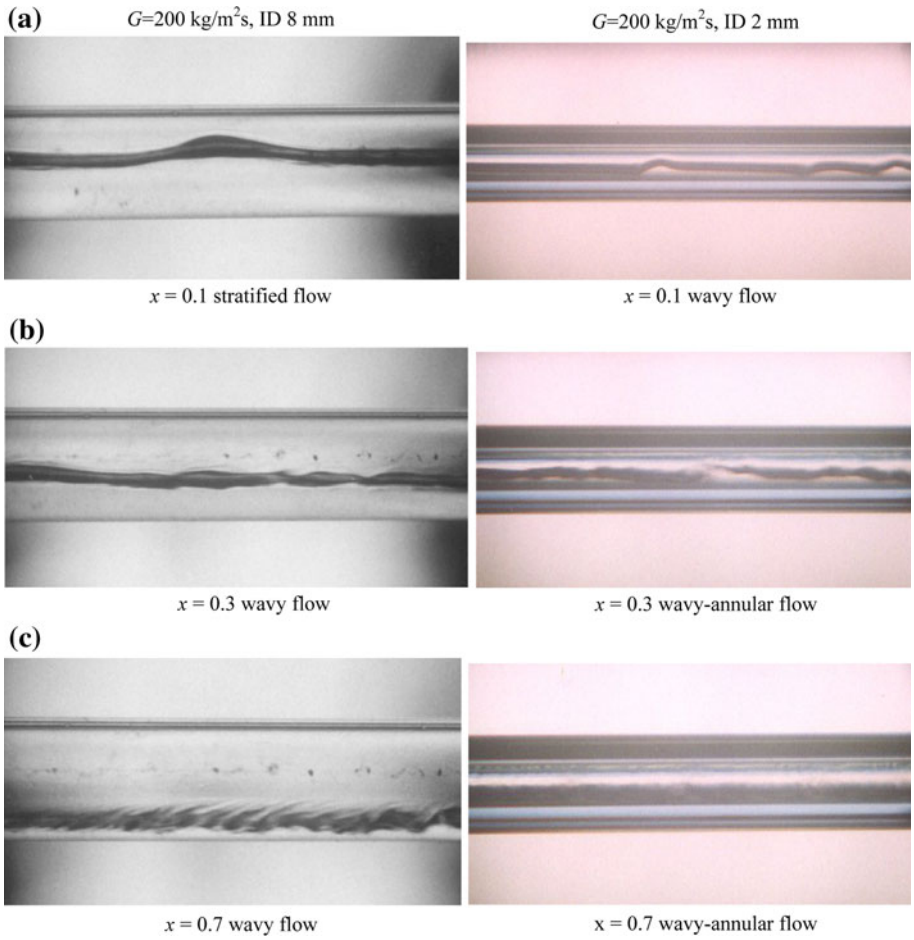

Fig. 4 Experimental flow patterns for R-134a in 2 and 8 mm tube

and annular flow is predominant. This means that a saturated vapor enters at $x = 1.0$ and goes directly into either the annular flow regime or wavy-annular flow regime.

Hence, as shown in Fig. 6, flow pattern data in 2 mm tube can not apply to the Mandhane's flow pattern map proposed in large diameter tubes. Because this map does not consider the flow characteristics for acceleration phenomenon and phase change of fluid in the small diameter tube.

3.1.2.2 Taitel and Dukler's flow pattern map Figure 7 presents the flow pattern map evaluated for R-134a in internal diameter tube of 2 mm, plotted on the flow pattern map of Taitel and Dukler [30]. In Fig. 7, Taitel and Dukler [30]'s map agrees well with the experimental data of wavy-annular flow and annular flow, but does not agree with wavy flow. This is because the quality for transition of wavy flow in 2 mm tube is lower than that in 8 mm tube. This reason results in lower F value, as shown in Fig. 7.

From above results, their map did consider the effect of tube diameter and fluid property, but did not consider the flow pattern in a small diameter tube. Therefore, we must carefully consider when applying the experimental data in the small diameter tube to Taitel and Dukler [30]'s map.

3.1.2.3 Dobson's flow pattern map Figure 8 shows the observed evaporation flow pattern in 8 mm tube plotted on the Dobson' map which is proposed in a horizontally smooth tube of 4.57 mm. The large difference between the experimental data and Dobson' map occurs at lower quality ($x < 0.4$) and higher mass flux ($G > 200$ kg m^{-2} s^{-1}).

Figure 9 presents the comparison of the experimental data in 2 mm with Dobson' flow pattern map. As shown in Fig. 9, Dobson' map agree with the experimental data and lower quality ($x = 0.1$). This is because his map is proposed for evaporation flow pattern in 4.57 mm tube.

3.2 Evaporation heat transfer

3.2.1 Effect of vapor quality and tube diameter

Figures 10 and 11 present the local evaporation heat transfer coefficients as a function of vapor quality for R-22

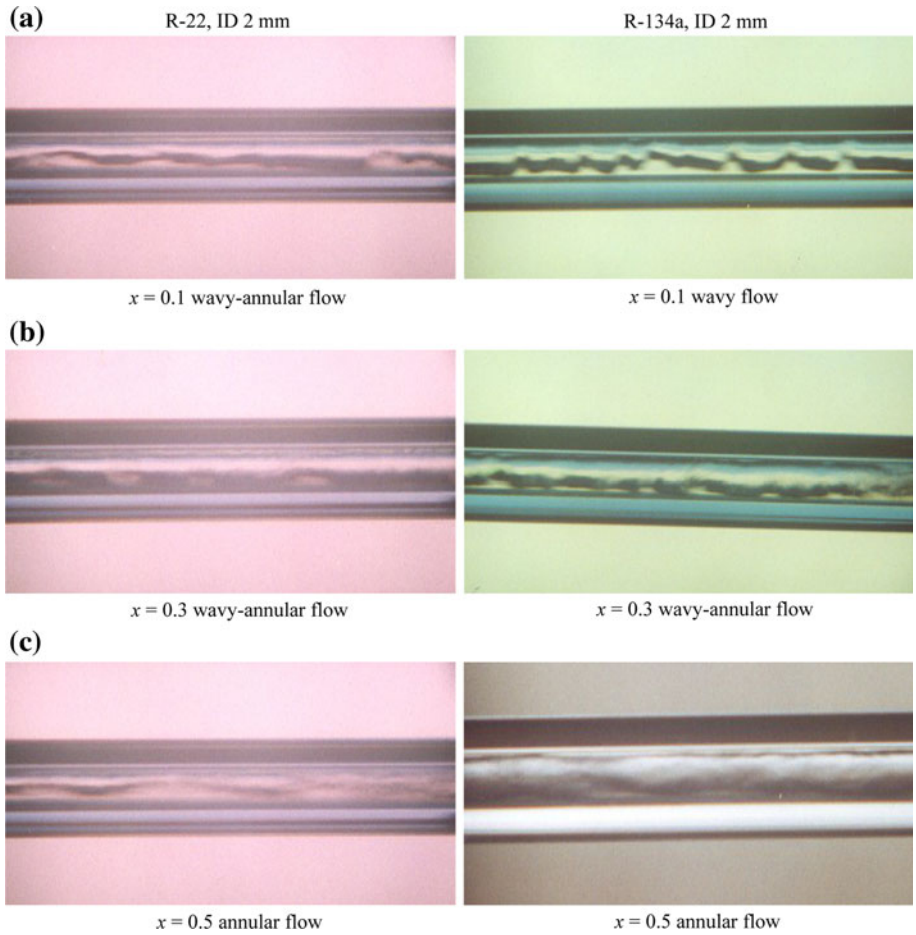

Fig. 5 Experimental flow patterns for R-22 and R-134a at $G = 400$ kg m^{-2} s^{-1} in 2 mm tube

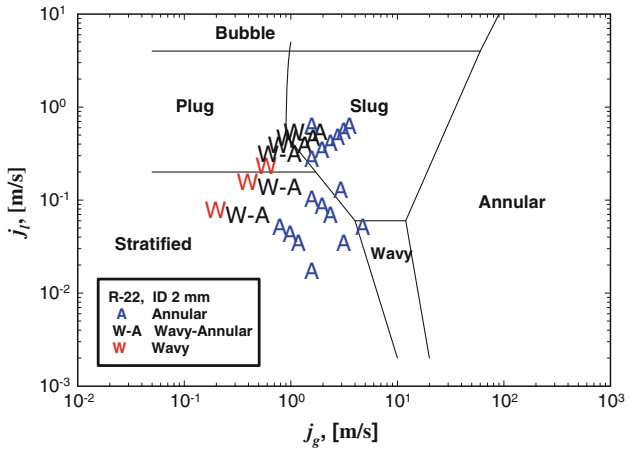

Fig. 6 Comparison of experimental flow patterns with Mandhane's flow pattern map in 2 mm tube

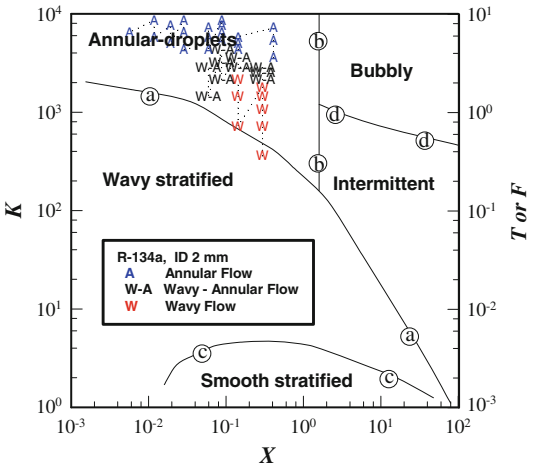

Fig. 7 Comparison of experimental flow patterns with Tailtel and Dulker's flow pattern map in 2 mm tube

in inner tube diameters of 3.36 and 5.35 mm and for R-134a in inner tube diameters of 1.77 and 3.36 mm, respectively. As shown in the Figs. 10 and 11, smaller inner diameter tube shows higher heat transfer coefficient, especially, at the high quality region of $x > 0.5$. The heat transfer coefficient of R-22 in 3.36 mm is about 15% higher than that in 5.35 mm, and the heat transfer coefficient of R-134a in 1.77 mm is about 20% higher than that in 3.36 mm.

These results agree with an experiment carried out by Yan and Lin [13, 37] to study the evaporation heat transfer of R-134a inside diameter tube of 2.0 mm. They reveal that

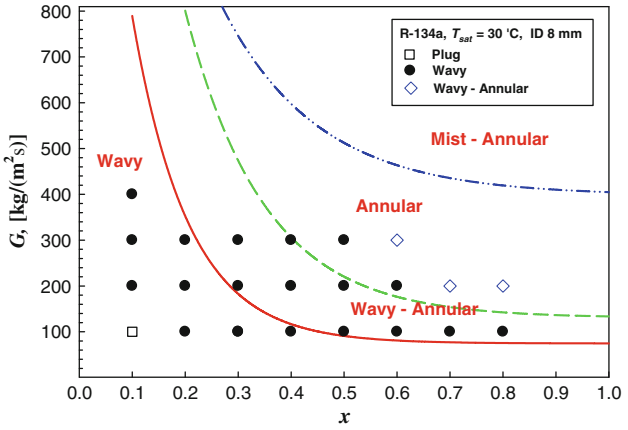

Fig. 8 Comparison of experimental flow patterns with Dobson's flow pattern map in ID 8 mm tube

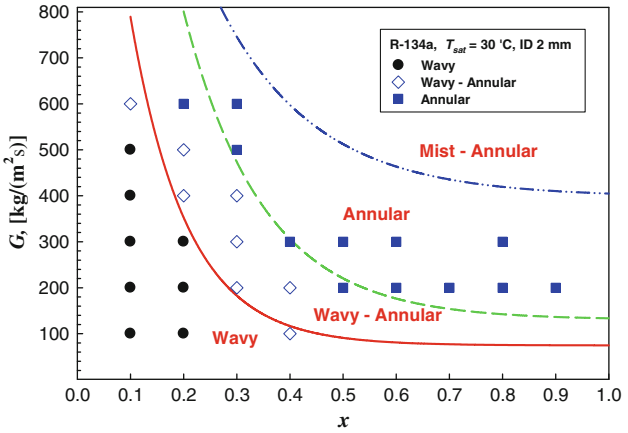

Fig. 9 Comparison of experimental flow patterns with Dobson's flow pattern map in ID 2 mm tube

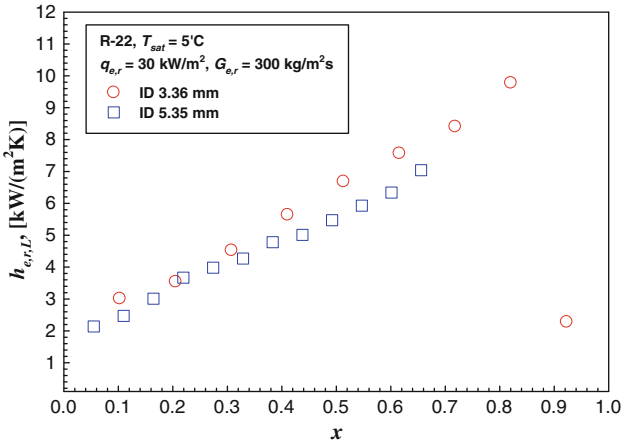

Fig. 10 Comparison of local evaporation heat transfer coefficients with vapor quality inside diameter tubes of 3.36 and 5.35 mm

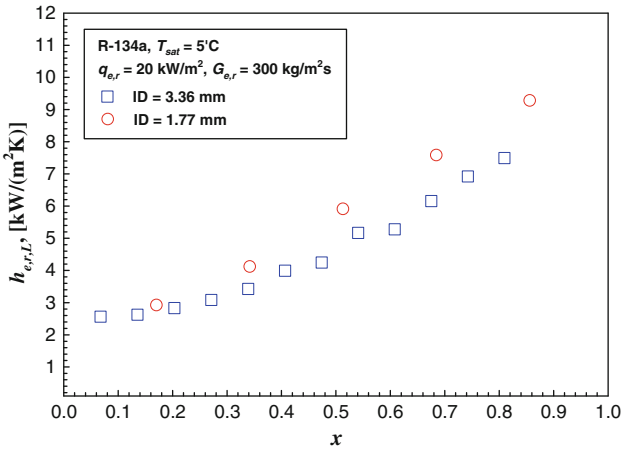

Fig. 11 Comparison of local evaporation heat transfer coefficients with vapor quality inside diameter tubes of 1.77 and 3.36 mm

the evaporation heat transfer in the small pipes was significantly higher than that in large tubes.

It can be seen that this results from the thinner liquid film of annular flow and fast transition from stratified flow or wavy flow to annular flow in smaller diameter tubes, as mentioned in Sect. 3.1. Through the experiment for evaporation flow patterns, it has been observed the liquid film thickness of annular flow in 2 mm were thinner than that in 8 mm, and transitions from stratified flow or wavy flow to annular flow in 2 mm were also faster than that in 8 mm [38].

Similarly, Sumith et al. [39] measured the saturated flow boiling heat transfer and pressure drop of water in a stainless steel tube with an inner diameter of 1.45 mm. They indicated that thinner liquid film evaporation dominated the heat transfer in the tube.

As shown in the Figs. 10 and 11, the local evaporation heat transfer coefficient increases evidently with vapor quality in three tubes. Especially, the increase of heat transfer coefficient is distinct at the ranges from 0.5 to 0.8. This is due to a more active convective boiling and the increasing contact surface area of heat transfer in this region.

3.2.2 *Effect of heat flux*

Figures 12, 13, 14 show the variation of the local evaporation heat transfer coefficients with heat fluxes at the higher quality region for R-134a in 5.35 mm, for R-22 in 3.36 mm and for R-22 in 1.77 mm, respectively. At the low quality region of $x < 0.3$, the heat transfer coefficient in three tubes increases hardly with increasing heat flux. This is probably due to a persistence of the nucleate boiling contribution. This trend agrees with the experimental results by Rossi et al. [40].

But the influence of the refrigerant heat flux appear in the high vapor quality range of $x > 0.5$. The local heat

transfer coefficient in this region increases about 18%, due to an increase of convective boiling. Nucleate boiling is suppressed at high quality where the effect of heat flux on heat transfer coefficient becomes lower.

As shown in Figs. 12, 13, 14, a dryout inception appears with higher heat flux and smaller tube. At dryout inception, the annular film starts breaking up, causing the heat transfer coefficient to rapidly decrease to low values typical of mist regime, at dryout completion, where the liquid film is completely vanished. From this point up to a vapor quality of 1, the flow is mainly constituted of vapor with subsisting droplets in its core, therefore depicting low heat transfer coefficients. The dryout completion in this test conditions did not appear.

In Fig. 14, the quality for dryout inception is lower as heat flux increases. This is because the inception and completion of annular flow is at a lower quality due to increasing heat flux. Another reason is that the convective boiling contribution increases due to higher heat flux.

3.2.3 *Effect of mass flux*

Figure 15 shows the effect of mass flux on heat transfer coefficient for R-22 in 3.36 mm tube. The variation from 300 to 500 kg m^{-2} s^{-1} represents an increase of 20–40%. At the low vapor quality region of $x < 0.4$, the heat transfer coefficient increases about 20%. Since at low vapor qualities the mass flux influence is so small, it can be concluded that in this region convective boiling contribution is small and therefore nucleate boiling is dominant. While at the high vapor quality range of $x < 0.4$, the heat transfer coefficient increases about 40%. It is clear that this increase is due to the mass flux influence, by means of the Reynolds number, on the convective boiling contribution.

For the higher mass flux in the convective boiling region, the increase in the heat transfer coefficient appears

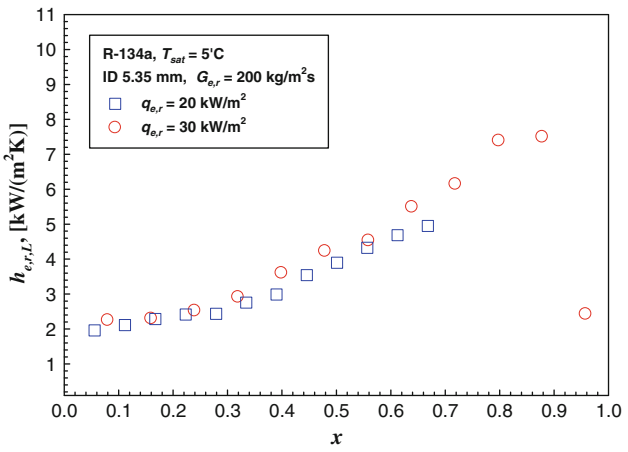

Fig. 12 Comparison of local evaporation heat transfer coefficients with heat flux in inner diameter tube of 5.35 mm

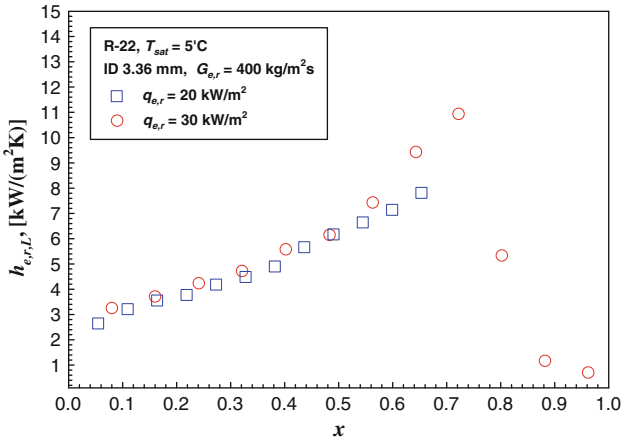

Fig. 13 Comparison of local evaporation heat transfer coefficients with heat flux in inner diameter tube of 3.36 mm

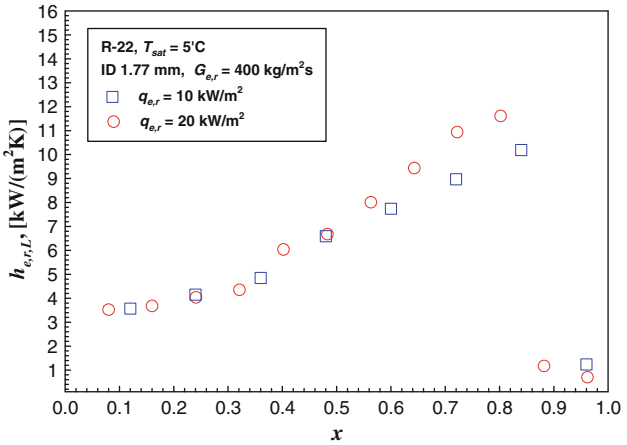

Fig. 14 Comparison of local evaporation heat transfer coefficients with heat flux in inner diameter tube of 1.77 mm

at a lower quality, which can be explained by the dominant annular flow with increasing quality.

Nucleate boiling suppression appears earlier for the higher mass flux, which means that convective heat transfer appears earlier under the higher mass flux condition. The lower mass flux results show smaller increases in the heat transfer coefficient in the convective region.

The heat transfer coefficients suddenly increase in the annular flow region before the dryout inception, which can be explained that as the quality increased in annular flow, the effective wall superheat decreases due to the thinner liquid film or less thermal resistance in the liquid film.

At the dryout inception and for the higher mass flux condition, the heat transfer coefficient is decreased. This is because the dryout inception vapor quality decreases with increasing heat flux, that is, dryout occurs earlier with regards to the vapor quality. Thus, the heat transfer coefficient at the dryout boundary decreases. For the lower mass flux condition there is no such trend, which could

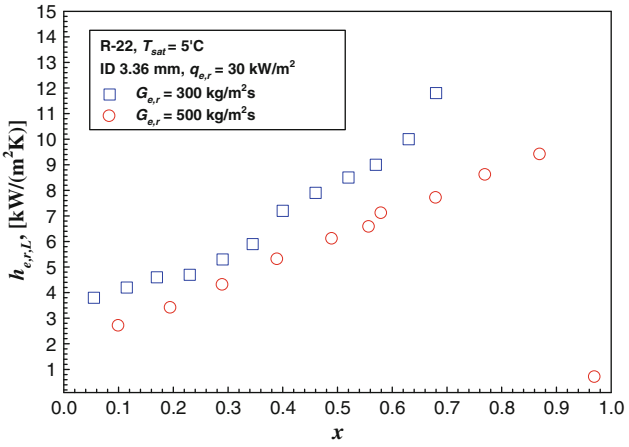

Fig. 15 Comparison of local evaporation heat transfer coefficients with mass flux in inner diameter tube of 3.36 mm

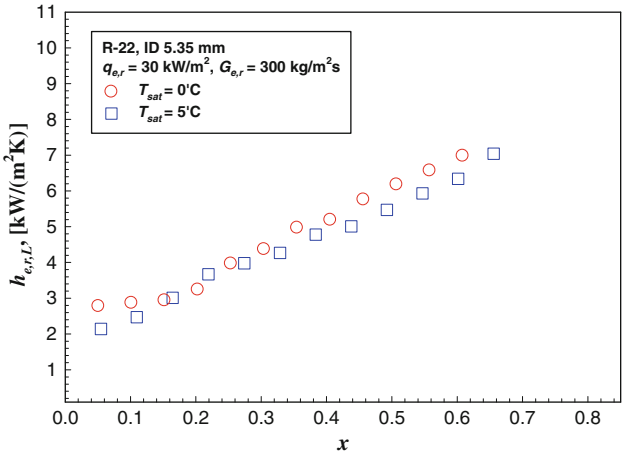

Fig. 16 Comparison of local evaporation heat transfer coefficients with saturation temperature in inner diameter tube of 5.35 mm

possibly be due to a combined function of both mass flux and heat flux.

3.2.4 *Effect of saturation temperature*

It is known that the variation of saturation temperature changes the physical properties (density, thermal conductivity, specific heat and dynamic viscosity) and flow patterns of the refrigerant. Also, these variations have an effect on local evaporation heat transfer coefficient.

Figure 16 presents the local heat transfer coefficient for R-22 in 5.35 mm tube at the different saturation temperatures of 0 and 5°C. At the same quality, the heat transfer coefficient increases with decreasing saturation temperature across the range of quality. This is because the heat transfer rate might be reduced by the lower vapor shear due to a decrease in vapor velocity at the vapor–liquid interface occurring at higher temperatures.

Another proposed reason is that heat transferred through the liquid annulus in annular flow pattern depends on the thermal conductivity of liquid film, and that the liquid refrigerant film at 10°C has a lower thermal conductivity than at 5°C.

This results in a decrease of the heat transfer coefficient as the saturation temperature is increased. These results are similar to previous studies reported by Agostini and Bontemps [41], Shiferaw et al. [42] and Lie et al. [43].

3.3 Comparison of experimental data with existing correlations

It is important to compare the present data in small diameter tubes to the previous correlations. In this paper, the heat transfer coefficients of the present study were analyzed and compared using seven previous heat transfer coefficient correlations proposed by Shah [44], Jung et al. [45], Gungor and Winterton [9], Liu and Winterton [46], Oh et al. [3], Wattelet et al. [47] and Yan and Lin [13]. Table 5 shows the deviation percentage of the comparison.

Overall, the Oh et al. [3] correlation gives the best prediction of all seven. Among several existing correlations, the correlations of Liu and Winterton [46] and Wattelet et al. [47] give a relatively good prediction of heat transfer coefficient with reasonable mean deviations of −19.8 to −26.2%. But the correlations by Jung et al. [45], Shah [44], Gungor and Winterton [9] and Yan and Lin [13] show the large deviation because the correlations was developed using conventional tube. Yan and Lin proposed the experimental correlation using R-134a in 2 mm diameter tube. The correlation was developed with limited data. So it is not useful for heat transfer prediction. As shown in Table 5, the comparison with all correlations shows a higher deviation for the smaller tube due to a higher heat transfer coefficient.

The previous correlations generally underestimate the experimental data. This is because the previous correlations fail to predict a convection heat transfer for evaporating refrigerants in small diameter tubes. Therefore, it is careful considered to apply the previous correlations proposed in large tubes to evaporation heat transfer in small diameter tubes.

3.4 Development of a new correlation

As the results of comparison with evaporation heat transfer coefficients for three small diameter tubes to various correlations, it is clear that the deviation between experimental data and the existing correlations is quite large. So, a new heat transfer correlation based on the experimental data is necessary, and the new correlation which is a form of Oh et al. [3]'s one was proposed in the present study. It concluded that Oh et al. [3]'s correlation can predict well the evaporation heat transfer characteristics of R-22 and R-134a with respect to the variation of tube diameter.

Table 5 The deviations between the calculated and experimental Nusselt number

$\sigma_{avg} = \left\{\sum_{i=1}^{n}\left(\frac{Nu_{cal,i}-Nu_{\exp,i}}{Nu_{\exp,i}}\right)/N\right\} \times 100$, $\sigma_{abs} = \left\{\sum_{i=1}^{n}\left|\frac{Nu_{cal,i}-Nu_{\exp,i}}{Nu_{\exp,i}}\right|/N\right\} \times 100$

Author	Refrigerant			
	R-22		R-134a	
	σ_{avg}	σ_{abs}	σ_{avg}	σ_i
Wattelet et al.				
$d_i = 1.77$ mm	−26.2	36.1	−26.8	27.8
$d_i = 3.36$ mm	−24.6	33.7	−23.3	24.3
$d_i = 5.35$ mm	−21.6	30.4	−21.7	22.8
Gungor and Winterton				
$d_i = 1.77$ mm	−42.1	45.2	−34.3	34.6
$d_i = 3.36$ mm	−41.6	44.5	−33.1	33.1
$d_i = 5.35$ mm	−39.7	39.7	−32.4	32.4
Shah				
$d_i = 1.77$ mm	−54.7	54.7	−50.8	50.8
$d_i = 3.36$ mm	−48.8	48.8	−47.8	47.8
$d_i = 5.35$ mm	−46.2	46.2	−45.2	−45.2
Jung et al.				
$d_i = 1.77$ mm	−36.4	40.8	−35.2	36.1
$d_i = 3.36$ mm	−35.5	40.3	−33.7	33.7
$d_i = 5.35$ mm	−32.8	32.8	−24.3	27.6
Liu and Winterton				
$d_i = 1.77$ mm	−22.3	32.4	−18.6	24.7
$d_i = 3.36$ mm	−21.8	31.2	−17.5	23.6
$d_i = 5.35$ mm	−19.8	29.4	−15.8	22.4
Yan and Lin				
$d_i = 1.77$ mm	62.3	65.1	60.2	61.3
$d_i = 3.36$ mm	57.0	58.4	48.5	59.3
$d_i = 5.35$ mm	55.6	58.1	46.1	57.4
Oh et al.				
$d_i = 1.77$ mm	−14.3	27.6	13.2	26.6
$d_i = 3.36$ mm	−12.8	24.8	11.8	23.5
$d_i = 5.35$ mm	−11.6	19.7	9.9	20.2

As discussed earlier, the flow pattern in small diameter tubes is dominantly the annular flow. For the annular flow regime, many researchers have correlated convective evaporation data by assuming that the ratio of the two-phase Nusselt number to the Nusselt number predicted by a single phase correlation (based on the superficial liquid Reynolds number) is exclusively a function of the Martinelli parameter.

The theoretical basis for this hypothesis is based on an analogy of heat transfer to momentum transfer, which is also assumed in more theoretical annular flow models when one assumes that the turbulent Prandtl number is a constant. Utilizing the correlation of Dittus–Boelter to predict the single-phase Nusselt number, regression analysis of our experimental data yielded the following form:

$$Nue = 0.034\mathrm{Re}l^{0.8}\,\mathrm{Pr}\,l^{0.3}fe(X_{tt}) \tag{7}$$

where

$$fe(X_{tt}) = \left[1.58\left(\frac{1}{X_{tt}}\right)^{0.87}\right] \tag{8}$$

The function $f_e(X_{tt})$ at the end of Eq. 7 represents the two-phase multiplier. The applicable ranges of the new proposed correlation (Eq. 7) are as follows:

$$1.8 \le \left(\frac{1}{X_{tt}}\right) \le 40, \quad 1.5 \le d_i \le 6,$$
$$200 \le G_{e,r} \le 600, \quad 0.15 \le 0.85, \quad 10 \le q_{e,r} \le 30$$
$$1000 \le \mathrm{Re}_l \le 20000, \quad 2 \le \mathrm{Pr}_l \le 5$$

Comparison of the proposed heat transfer correlation with all present measured data is shown in Fig. 17. The proposed correlation predicted the experimental data very well with Martinelli parameter. The new correlation shows a good agreement with the mean deviation of 2.4%.

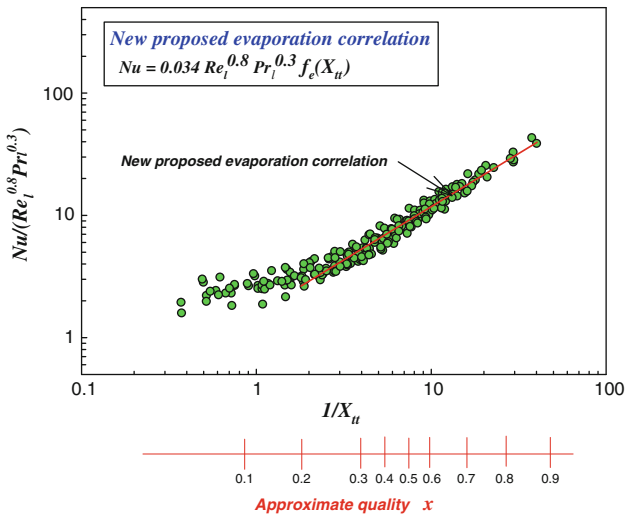

Fig. 17 Comparison of experimental *Nu* and calculated Nu_e using the new proposed evaporation correlation

4 Conclusions

Evaporating flow patterns and heat transfer coefficients for R-22 and R-134a were measured in small diameter tubes of 1.77, 3.36 and 5.35 mm. The following conclusions were acquired from the experiment.

(1) In flow patterns during evaporation, annular flows in 2 mm tube occurred at the relatively lower mass quality comparing to 8 mm tube. The flow patterns in 2 mm tube have been fairly discordant with the Mandhane's flow pattern maps.

(2) The evaporation heat transfer characteristics in the small diameter tubes ($d_i < 6$ mm) were observed to be strongly affected by inner diameter change and to differ from those in the large diameter tubes. The local evaporating heat transfer coefficients of 3.36 mm tube is about 15% higher than those of 5.35 mm tube, and the evaporating heat transfer coefficients of 1.77 mm tube is about 20% higher than those of 3.36 mm tube.

(3) Most of the existing correlations which were proposed in the large diameter tube failed to predict condensation heat transfer. And also, recently proposed Yan and Lin correlation is not enough to consider the heat transfer characteristics for small diameter tube. Therefore, it is necessary to develop accurate and reliable correlation in small diameter tubes to predict heat transfer characteristics in the small diameter tubes. So the new condensation heat transfer correlation based on the experimental data is proposed in the present study.

References

1. Webb RL, Zhang M, Narayanamurthy R (1998) Condensation heat transfer in small diameter tubes. In: Proceedings of 11th IHTC, vol 6, pp 403–408, Kyongju
2. Oh HK, Hong JW (1999) Condensing heat transfer characteristics of alternative refrigerants in small diameter tubes. J SAREK 28(5):396–402
3. Oh HK, Katsuta M, Shibata K (1998) Heat transfer characteristics of R134a in a capillary tube heat exchanger. In: Proceedings of 11th international heat transfer conference, vol 6, pp 131–136
4. Tran TN, Wambsganss MW, France DM (1996) Small circular- and rectangular-channel boiling with two refrigerants. Int J Multiph Flow 22(3):485–498
5. Bao ZY, Fletcher DF, Haynes BS (2000) Flow boiling heat transfer of Freon R11 and HCFC123 in narrow passages. Int J Heat Mass Transf 43(18):3347–3358
6. Haynes BS, Fletcher DF (2003) Subcooled flow boiling heat transfer in narrow passages. Int J Heat Mass Transf 46(19): 3673–3682
7. Zhang W, Hibiki T, Mishima K (2004) Correlation for flow boiling heat transfer in mini-channels. Int J Heat Mass Transf 47:5749–5763
8. Chen JC (1996) A correlation for boiling heat transfer to saturated fluids in convective flow. I&EC Proc Des Dev 5:322–329
9. Gungor KE, Winterton RHS (1986) A general correlation for flow boiling in tubes and annuli. Int J Heat Mass Transf 29(3):351–358
10. Kandlikar SG (2004) Heat transfer mechanisms during flow boiling in microchannels. ASME J Heat Transf 126(1):8–16
11. Choi KI, Pamitran AS, Oh CY, Oh JT (2007) Boiling heat transfer of R-22, R-134a, and CO_2 in horizontal smooth minichannels. Int J Refrig 30(8):1336–1346
12. Choi KI, Pamitran AS, Oh CY, Oh JT (2008) Two-phase pressure drop of R-410A in horizontal smooth minichannels. Int J Refrig 31(1):119–129
13. Yan YY, Lin TF (1998) Evaporation heat transfer and pressure drop of refrigerant R-134a in a small pipe. Int J Heat Mass Transf 41(24):4183–4194
14. Fujita Y, Yang Y, Fujita N (2002) Flow boiling heat transfer and pressure drop in uniformly heated small tubes. In: Proceedings of the twelfth international heat transfer conference, vol 3, pp 743–748
15. Kim MH, Lee SY, Mehendale SS, Webb RL (2003) Microchannel heat exchanger design for evaporator and condenser applications. Adv Heat Transf 37:297–429
16. Ghiaasiaan SM, Abdel-khalik SI (2001) Two-phase flow in microchannels. Adv Heat Transf 34:145–254
17. Thome JR (2004) Boiling in microchannels: a review of experiment and theory. Int J Heat Fluid Flow 25(2):128–139
18. Sobhan CB, Garimella SV (2001) A comparative analysis of studies on heat transfer and fluid flow in microchannels. Microscale Thermophys Eng 5(4):293–311
19. Kandkikar SG (2002) Two-phase flow patterns, pressure drop, and heat transfer during boiling in minichannel flow passages of compact evaporators. Heat Transf Eng 23(1):5–23
20. Watel B (2003) Review of saturated flow boiling in small passages of compact heat-exchangers. Int J Therm Sci 42(2):107–140
21. Yun R, Heo JH, Kim Y (2006) Evaporative heat transfer and pressure drop of R-410A in micro-channels. Int J Refrig 29(1):92–100
22. Lee J, Mudawar I (2005) Two-phase flow in high heat-flux microchannel heat sink for refrigeration cooling applications: part II—heat transfer characteristics. Int J Heat Mass Transf 48(5): 941–955

23. Cavallini A, Del Col D, Doretti L, Matkovic M, Rossetto L, Zilio C (2005) Two-phase frictional pressure gradient of R236ea, R-134a and R-410A inside multi-port mini-channels. Exp Therm Fluid Sci 29(7):861–870
24. Vlasie C, Macchi H, Guilpart J, Agostini B (2004) Flow boiling in small diameter channels. Int J Refrig 27(2):191–201
25. Lemmon EW, Huber ML, McLinden MO (2007) Reference fluid thermodynamic and transport properties (REFPROP), Version 8.0. In: NIST Standard Reference Database 23. National Institute of Standard and Technology, Gaithersburg, MD, USA
26. Moffat RJ (1998) Describing the uncertainties in experimental results. Exp Therm Fluid Sci 1(1):3–17
27. Baker O (1954) Design of pipelines for simultaneous flow of oil and gas. Oil Gas J 53:185–195
28. Scott DS (1963) Properties of cocurrent gas–liquid flow. Adv Chem Eng 4:199–277
29. Mandhane JM (1974) A flow pattern map for gas-liquid flow in horizontal pipes. Int J Multip flow 1(4):537–554
30. Taitel Y, Dukler AE (1976) A model for predicting flow regime transitions in horizontal and near horizontal gas liquid flow. AIChE J 22(2):43–55
31. Bennett AW, Hewitt GF, Kearsey HA, Keeys RKF, Lacey PMC (1966) Flow visualization studies of boiling at high pressure. In: Proceedings of the Institution of Mechanical Engineers, 184, Pt 3C-Boiling Heat Transfer, pp 260–270
32. Bergles AE, Lopina RF, Fiori MP (1967) Critical-heat-flux and flow pattern observation for low-pressure water flowing in tubes. Trans ASME Ser C 89-1:69–74
33. Wambsganss MW, Jendrzejczyk JA, France DM (1991) Two-phase flow patterns and transitions in a small, horizontal, rectangular channel. Int J Multip Flow 17(3):327–342
34. Dobson MK, Chato JC, Hinde DK, Wang SP (1994) Experimental evaluation of internal condensation of refrigerations R-12 and R-134a. ASHRAE Trans 5(3):744–754
35. Breber G, Palen JW, Taborek J (1980) Prediction of horizontal tube-side condensation of pure components using flow regime criteria. J Heat Transf 102:471–476
36. Tandon TN, Varma HK, Gupta CP (1982) A new flow regime map for condensation inside horizontal tubes. J Heat Transf 104:763–768
37. Yan YY, Lin TF (2003) Reply to Prof. R.L. Webb's and Dr. J.W. Paek's comments. Int J Heat Mass Transf 46(6):1111–1113
38. Oh HK, Hong JW (2002) Study on the flow characteristics of R-22, R-134a in small diameter tubes. Trans SAREK 14(9): 756–765
39. Sumith B, Kaminaga F, Matsumura K (2003) Saturated flow boiling of water in a vertical small diameter tube. Exp Therm Fluid Sci 27(7):789–801
40. De Rossi F, Mauro AW, Rosato A (2009) Local heat transfer coefficients and pressure gradients for R-134a during flow boiling at temperature between −9°C and +20°C. Energy Convers Manag 50(7):1714–1721
41. Agostini B, Bontemps A (2005) Vertical boiling of refrigerant R-134a in small channels. Int J Heat Fluid Flow 26(2):296–306
42. Shiferaw D, Huo X, Karayiannis TG, Kenning DBR (2010) Examination of heat transfer correlations and a model for flow boiling of R134a in small diameter tubes. Int J Heat Mass Transf 50(25–26):5177–5193
43. Lie YM, Su FQ, Lai RL, Lin TF (2006) Experimental study of evaporation heat transfer characteristics of refrigerants R-134a and R-407C in horizontal small tubes. Int J Heat Mass Transf 49(1–2):207–218
44. Shah MM (1982) Chart correlation for saturated boiling heat transfer equations and further study. ASHRAE Trans 88:185–196
45. Jung DS, McLinden M, Randermacher R, Didion D (1989) A study of flow boiling heat transfer with refrigerant mixtures. Int J Heat Mass Transf 32(9):1751–1764
46. Liu Z, Winterton RHS (1991) A general correlation for saturated and subcooled flow boiling in tubes and annuli, based on a nucleate pool boiling equation. Int J Heat Mass Transf 34(1): 2759–2766
47. Wattelet JP, Chato JC, Souza AL, Christoffersen BR (1994) Evaporative characteristics of R-12, R-134a, and a mixture at low mass fluxes. ASHRAE Trans 94-2-1:603–615